well as scientific examples taking advantage of this unique instrumentation.

ChemMatCARS Sector 15 is principally supported by the National Science Foundation/Department of Energy under grant number NSF/CHE-0822838. Use of the Advanced Photon Source was supported by the U. S. Department of Energy, Office of Science, Office of Basic Energy Sciences, under Contract No. DE-AC02-06CH11357.

1. Ilavsky, J., Jemian, P.R., Allen, A.J., Zhang, F., Levine, L.E. and Long, G.G. Journal of Applied Crystallography, 42, 2009, 469-479.
2. Ilavsky, J., Zhang, F., Allen, A.J., Levine, L.E. Jemian, P.R., and Long, G.G. Metallurgical and Materials Transactions A, Metallurgical and Materials Transactions A, 44, 2013,68-76.

Session II, Tuesday, September 10

L4

GISAXS – THEORY, EXPERIMENTAL REALIZATION AND SOME RESULTS

V. Holý

Department of Condensed Matter Physics, Faculty of Mathematics and Physics, Charles University in Prague, Ke Karlovu 5, 121 16 Praha, Czech Republic
holy@mag.mff.cuni.cz

In the last decades, various types of nanostructures have been intensively studied by physical, chemical and biological methods. Since the properties of nanostructures are substantially influenced by their structure, structural research of nanostructures is extremely important for the understanding of their performance. Under the structure of the nanoobjects we understand not only the atomic arrangement (the crystal structure in the case of crystalline objects), but more importantly the shapes, sizes and arrangement of individual nano-objects. Methods based on scattering (X-ray-, electron- or neutron scattering) consist in mapping of a part of reciprocal space, the size of which depends on the size of the nanoobjects. Small-angle X-ray scattering (SAXS) usually probes the reciprocal space up to distances of few reciprocal nm, i.e. the method can study particles of sizes from several nm up to approx. one micrometer. For nanoobjects dispersed on a surface or in a thin layer or multilayer, small-angle scattering method is usually performed in grazing incidence geometry (grazing-incidence small-angle x-ray scattering – GISAXS), in which specular scattering from the surface or from the interfaces in the host layer system plays important role.

The theoretical part of the talk will summarize the basic theoretical approaches describing the scattering process (kinematical approximation, distorted-wave Born approximation – DWBA), as well as several theoretical approaches describing self-organized systems on nanoparticles. Several software packages of GISAXS simulations available mostly free of charge will be introduced as well. The theory of GISAXS can be found in [1, 2].

In the second part of the talk the attention will be paid to several experimental realizations of a GISAXS measurement, including laboratory and synchrotron set-ups. The third part of the talk will focus to several experimental examples including mainly semiconductor quantum dots in epitaxial layered systems (Ge/Si, InAs/GaAs, PbSe/PbEuTe) and semiconductor and metallic nanocrystals in amorphous matrix (Ge/SiO_2, Ge/Al_2O_3, Co/SiO_2, among others).

1. U., Pietsch, V. Holý and T. Baumbach T., *High-Resolution X-Ray Scattering From Thin Films to Lateral Nanostructures*, Advanced Texts in Physics, Springer-Verlag Berlin, Heidelberg, New York 2004.
2. G. Renaud, R. Lazzari and F. Leroy, Surface Science Reports **64**, 255-380 (2009).

L5

GRAZING INCIDENCE X-RAY DIFFRACTION: STUDY OF DEPTH DISTRIBUTION OF CHEMICAL PHASE CONCENTRATION

E. Dobročka[1], P. Novák[2], M. Vallo[1], T. Lalinský[1]

[1]Institute of Electrical Engineering, Slovak Academy of Sciences, Dúbravská cesta 9, 841 04 Bratislava, Slovakia
[2]Institute of Nuclear and Physical Engineering, Faculty of Electrical Engineering and Information Technology, Slovak University of Technology, Ilkovičova 3, 812 19 Bratislava, Slovakia
edmund.dobrocka@savba.sk

Grazing incidence geometry is especially useful in X-ray diffraction analysis of thin films. The penetration depth of radiation can be easily changed by an appropriate selection of the angle of incidence that enables obtaining information from different depths of the sample. Approaching the critical angle $_c$ for total external reflection this depth can be decreased even to a nanometer scale. The method therefore provides an efficient tool for the analysis of depth distribution of various structural properties, such as the crystallite size, the amorphous fraction, stress or the concentration of chemical phase. While for most of these properties the absorption of the radiation can be characterized by an average attenuation coefficient , special care has to be paid to the last property. Variation of chemical phase concentration with depth usually results in depth dependence of the density and hence the attenuation coefficient. In the presented contribution a method for determination of depth distribution of a chemical phase is outlined. The method correctly takes into account the depth variation of the attenuation coefficient. The proposed method is verified on thin oxidized iridium layers. Three simple model cases are discussed and compared with the experimental results.

In the vicinity of critical angle the intensity of X-rays penetrating the homogeneous sample is exponentially damped according to relations [1]

$$I \quad I_0 \exp(\ 2xKB) \tag{1}$$

$$B \quad \sqrt{\frac{1}{2}\ \sqrt{(\ ^2\ \ 2\ )^2\ \ 4\ ^2}\ \ (\ ^2\ \ 2\ )} \tag{2}$$

where I_0 is the intensity of the incident beam, x is the depth coordinate, $K = 2$ is the magnitude of the wave vector, and are related to refractive index n = 1 - i and depend on the electron density $_e$ and the attenuation coefficient . When the composition of the layer changes with depth, the parameters $_e$, , , , and B become a function of x and the intensity at the depth x is given as

$$I_{inhom}(x,a) \quad I_0 \exp(\ 2K\ \int_0^x B(t)dt\ ) \tag{3}$$

In the simplest case the layer contains only two crystalline phases with the weight fractions w_1 and w_2, they are not necessarily complementary, i.e. $w_1 + w_2$ 1. If the thickness T of the analyzed layer is in the range of nanometers, one can neglect the absorption of the intensity of the diffracted beam and the total amount $A_j^{tot}(\ )$ of the j–th phase (j = 1, 2) detected by measuring at the angle is proportional to the integral

$$A_j^{tot}(\ ) \quad SC\ \int_0^T w_j(x)\exp(\ 2K\ \int_0^x B(t)dt\ )dx \tag{4}$$

The intensity of the incident beam I_0 is included in the scaling factor SC. It should be pointed out that the weight fractions $w_j(x)$ appear also in $B(x)$ through the weighted values of the parameters (x) and (x) according to the composition of the layer at the depth x.

The total weight fractions $W_1(\ )$ and $W_2(\ )$ of both phases are given simply as

$$W_1(\ ) \quad \frac{A_1^{tot}(\ )}{A_1^{tot}(\ )\ \ A_2^{tot}(\ )},$$
$$W_2(\ ) \quad \frac{A_2^{tot}(\ )}{A_1^{tot}(\ )\ \ A_2^{tot}(\ )}, \tag{5}$$

The values $W_1(\ )$ and $W_2(\ )$ can be directly compared with the results obtained experimentally by measurement at various angles and the profiles $w_1(x)$ and $w_2(x)$ can be determined by numerical procedure based on an appropriate model.

In order to verify the capability of the outlined approach very thin iridium layers deposited on sapphire/GaN/AlGaN system and subsequently annealed in oxidizing atmosphere at 500 °C were analyzed by X-ray diffraction. The thickness of the samples was determined by X-ray reflectivity measurement [2]. All measurements were performed in parallel beam geometry with parabolic Goebel mirror in the primary beam. The X-ray diffraction patterns were recorded in grazing incidence set-up with the angle of incidence = 0.3°, 0.4°, 0.5°, 0.6° and 1.5°. Two crystalline phases – Ir (PDF No. 03-65-1686) and IrO_2 (PDF No. 00-15-0870) were identified. Quantitative analysis of the measurements was performed by software TOPAS 3.0. The results are shown in the Figure 2 (black squares).

The experimental results were analyzed within the framework of three model structures of the oxidized Ir layer [3]. In the first model the weight fraction of IrO_2 decreases gradually from the highest value $w_{IrO_2}(0)$ 1 at the surface. The depth profile of $w_{IrO_2}(x)$ corresponds to complementary error function erfc(x/L) according to the ex-

pected oxygen diffusion from the surface. The weight fraction of iridium is w_{Ir} 1 w_{IrO_2} . The model has one free parameter – the diffusion length L. The second model consists of two sublayers Ir (bottom) and IrO_2(top) separated by an abrupt interface. The free parameter is the depth t of the interface. In the third model the Ir and IrO_2 layers are separated by an amorphous IrO_2 interlayer. The model has two free parameters – the depths t_1 and t_2 of the two interfaces.

The effect of the depth distribution of the phases on the intensity damping is shown in Figure 1. The curves are calculated for the mixture of Ir and IrO_2 according to the first model. Detailed analysis [3] showed that the first and the second model are not able to explain the large difference between the values of W_{IrO_2} – 0.78 and 0.27 measured at a = 0.3° and 1.5°, respectively. The third model was therefore accepted as the most appropriate. The parameters t_1 and t_2 were optimized by least square method. The best fit was achieved for the values t_1 = 1.05 nm and t_2 = 3.22 nm. The resulting dependence W_{IrO_2} ( ) is shown in Figure 2 (red curve).

1. M. Birkholz: *Thin film analysis by X-ray scattering*. Weinheim: Wiley-vch. 2006.
2. M. Vallo, T. Lalinský, E. Dobročka, G. Vanko, A. Vincze, I. Rýger, *Appl. Surf. Sci.*, **267**, (2013), 159.
3. P. Novák, *Určenie hĺbkového profilu fázového zloženia tenkých vrstiev pomocou rtg difrakcie pri malom uhle dopadu*, Diploma thesis, FEI STU, Bratislava, (2012).

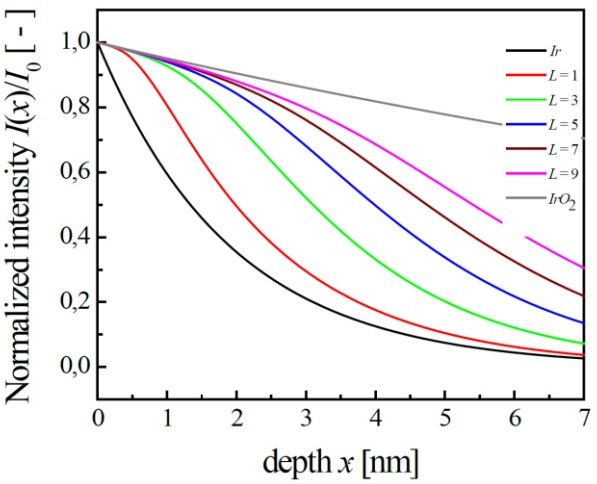

Figure 1. Normalized intensity as a function of depth x calculated for various diffusion lengths L (in *nm*). The black and grey curves correspond to pure Ir and IrO_2, respectively The angle of incidence = 0.5 .

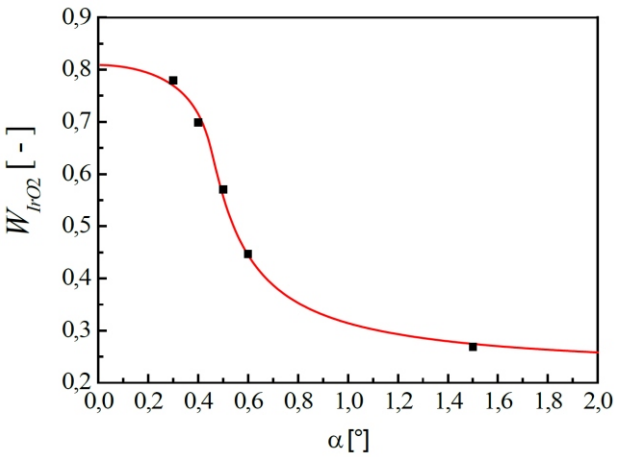

Figure 2. Experimental (black squares) and calculated values (red curve) of the total weight fraction W_{IrO_2} of IrO_2 phase as a function of angle of incidence .

L6

GISAXS APPLICATION TO A STUDY OF THE NANOPARTICLE SELF-ASSEMBLY AT THE AIR-WATER INTERFACE

M. Jergel[1], P. Šiffalovič[1], K. Vegso[1], M. Benkovičová[1], E. Majková[1], K. Nygard[2], O. Konovalov[3]

[1]Institute of Physics SAS, Dúbravská cesta 9, 845 11 Bratislava, Slovakia
[2]Dept. Chemistry & Mol. Biology, University Göteborg, 412 96 Göteborg, Sweden
[3]European Synchrotron Radiation Facility, BP 220, 38043 Grenoble, France
matej.jergel@savba.sk

Keywords: nanoparticles, GISAXS, Langmuir film

Abstract

An *in-situ* study of the colloidal silver nanoparticle self-assembly into a close-packed monolayer at the air/water interface followed by a 2D to 3D transition was performed by a fast tracking GISAXS technique in a Langmuir-Blodgett trough. Monitoring the immediate response of the system to the barrier movement enabled us to identify all relevant self-assembly stages including those far from the equilibrium. A new non-equilibrium phase before the monolayer collapse was found that is inaccessible by the competing direct space imaging techniques such as the scanning and transmission electron microscopies.

Introduction

Self-assembled arrays of chemically synthesized monodisperse nanoparticles are attractive for many novel and emerging applications. For example, the nanoparticle templates of plasmonic gold or silver nanoparticles provide a key to enhanced power conversion efficiency of future solar cells or may serve as unique substrates for the surface enhanced Raman scattering spectroscopy. The self-assembly takes place on the water surface in the Langmuir-Blodgett (LB) trough where a nanoparticle Langmuir film is formed and subsequently transferred onto a solid substrate. Macroscopic physical quantities such as the surface pressure, refractive index or surface potential of the nanoparticle Langmuir film are readily measureable while the conventional direct space imaging methods such as the scanning and transmission electron microscopy or nanoscale scanning probe techniques are inapplicable at the air/water interfaces due to the high vapour pressure and surface tension of the water subphase. Here, the reciprocal space techniques based on the scattering of X-rays or neutrons, in particular the synchrotron based grazing-incidence small-angle X-ray scattering (GISAXS), prove to be unique in revealing the atomic or molecular structure details at the air/water interface. We report here on the principal stages of a plasmonic nanoparticle Langmuir film compression at the air/water interface followed by a pressure release. The immediate film response to the surface pressure evolution is monitored *in situ* by a fast tracking GISAXS technique in order to detect transient phenomena far from the equilibrium. The structure evolution at nanoscale is related to the macroscopic behaviour monitored by the surface pressure, Brewster microscopy and imaging ellipsometry.

Experimental details

We studied Langmuir film composed of spherical Ag nanoparticles capped with oleic acid and oleylamine surfactant. The chemical synthesis was published elsewhere [1]. The surfactant prevents the nanoparticles from agglomeration. The diameter of the Ag nanoparticle core of 7 ± 0.7 nm was determined by SAXS. The Ag nanoparticle solution in chloroform of 0.2 mg/ml concentration was spread on the deionised water subphase (specific electrical resistance >18 M .cm) in a custom designed LB trough. After spreading the nanoparticles, the solvent was let to evaporate for 15 minutes before the measurement started. The *in situ* GISAXS measurements at the air/water interface during the barrier movement in the LB trough were performed at ID10B beamline at ERSF, Grenoble. The X-ray beam of the 300 100 m^2 size and 8 keV energy hit the air/water interface at 0.35ş grazing angle. A fast 2D X-ray detector PILATUS 300K was used. The reciprocal space calibration was done by the silver behenate standard. The Brewster angle microscopy and null ellipsometry images were obtained by an optical microscope with digital output (Hitachi) and imaging ellipsometer (Accurion), respectively.

Results and discussion

To track in situ the evolution of the nanoparticle order as a function of the surface pressure in the Langmuir trough during the compression and expansion at a constant barrier speed of 26 cm^2/min, a continuous series of the GISAXS frames was recorded as a movie. The time between the two successive frames of 1.87 s was short enough not to miss any relaxation effect, hence, the immediate response was monitored. The Fig. 1 shows the GISAXS patterns of the nanoparticle Langmuir film before and after the compression. They consist of the nanoparticle interference function modulated by the nanoparticle form factor. The q_z and q_y are the normal and lateral (in-plane) scattering vector components with respect to the air/water interface. The 1st order Bragg rods suggest presence of an ordered nanoparticle monolayer while the null ellipsometry image (Fig. 2) shows that it is discontinuous at small surface pressure. Considering the hexagonally ordered close-packed spherical nanoparticles, the lattice spacing before compression reads d_{10} 2 / $q_y^{\max}$ which for the first Bragg rod maxi-

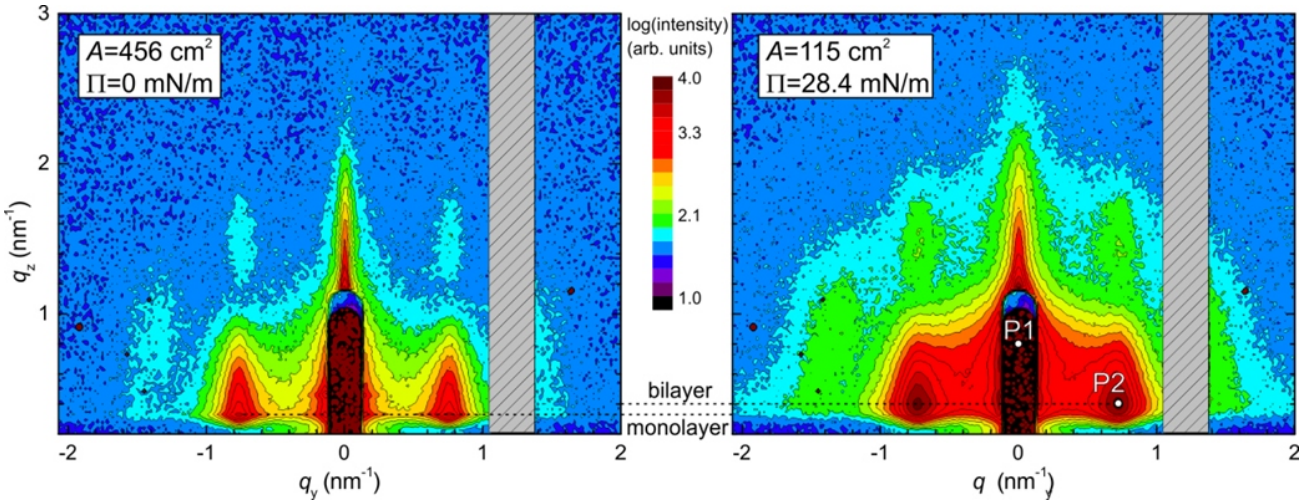

Figure 1. The GISAXS patterns of the nanoparticle Langmuir film at the surface pressure 0 mN/m (left) and 28.4 mN/m (right). The peaks P1 and P2 are associated with the AB stacked bilayer (see the text). The dead area between the detection modules of PILATUS 300K detector is hatched.

mum position $q_y^{max} = 0.75$ nm^{-1} gives the nearest-neighbour interparticle distance $2d_{10}/\sqrt{3} = 9.7$ nm. Assuming the mean nanoparticle core diameter of 7 nm from SAXS, this gives some 1.4 nm for the surfactant shell thickness. The compression results in an intensity redistribution along q_y of the central and 1st Bragg rods (Fig. 1). On the former, the maximum intensity shifts from the critical exit angle (Yoneda peak) to peak P1 (hidden by the specular beam stop) after compression which indicates the nanoparticle layering. On the latter, peak P2 evolves at the position that suggests formation of a vertically correlated second layer [2]. In particular, the AB stacking (hexagonal close-packed bilayer) is manifested by the diffraction peaks P1(q_y, q_z) and P2(q_y, q_z) located at (0, 2 /d_z) and (2 /d_{10}, /d_z), respectively, where the vertical lattice spacing d_z is given as $d_z \sqrt{6}/3$. Considering the in-plane interparticle distance = 9.7 nm, the calculated P2 peak position matches perfectly that one observed in the GISAXS pattern.

Based on the simultaneously measured pressure – area isotherm and GISAXS frames, we can identify four principal stages of the nanoparticle Langmuir film compression. In stage I, no measureable change in the surface pressure is detected (Fig. 3a). We observe self-assembly of nanoparticles evidenced by the presence of Bragg rods in GISAXS (Fig. 1) which happens presumably within isolated self-assembled nanoparticle islands as the null ellipsometry shows (Fig. 2). The nanoparticle islands coalesce gradually into larger assemblies during the compression as indicated also by the Brewster microscopy (not shown). The surface elastic modulus E calculated from

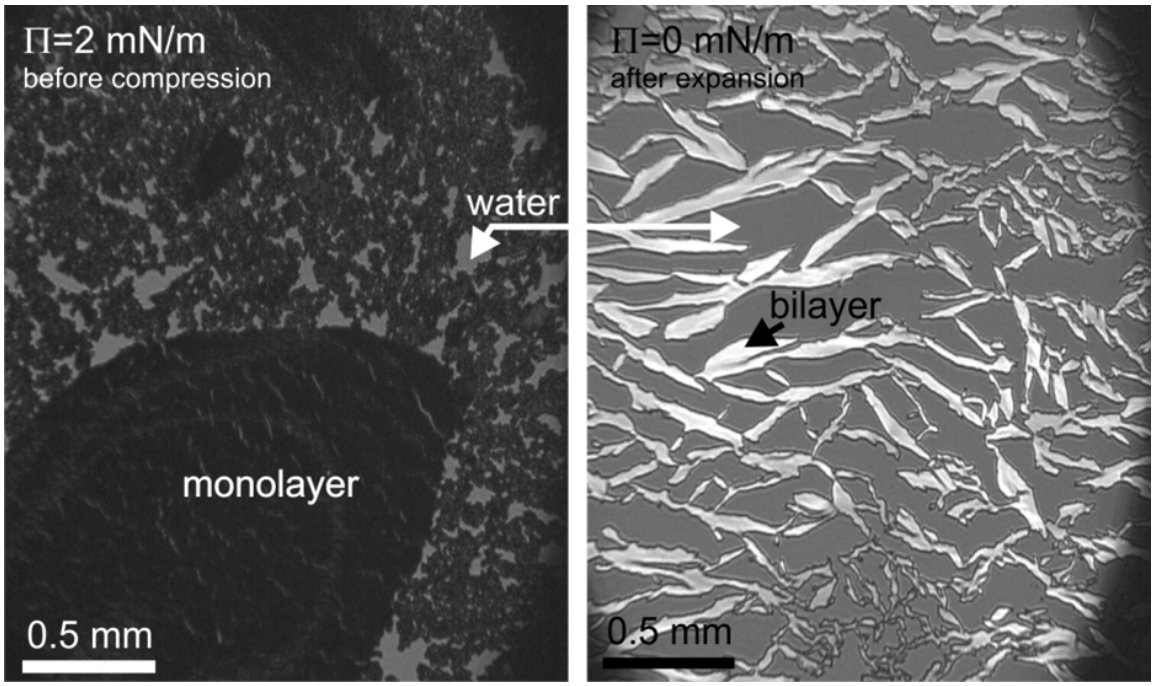

Figure 2. The null ellipsometry images of the nanoparticle Langmuir film before the compression (left) and after the expansion (right). The null imaging elipsometer was configured to stop the polarized light reflected from the nanoparticle monolayer.

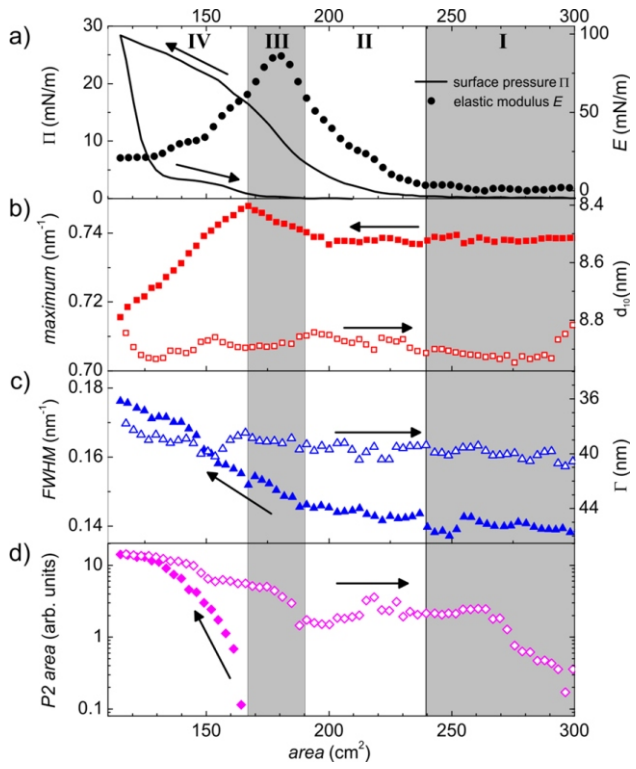

Figure 3. The major compression stages of the nanoparticle Langmuir film. The arrows show the compression and expansion periods. For a closer explanation see the text.

derivative (Fig. 3a) has no physical meaning for the freely floating isolated islands here. The reduction of the Bragg rod width (Fig. 3c) is not observed because of a restricted size of the coherently scattering domains in the pristine islands controlled by the nanoparticle cumulative disorder. In stage II, we observe a steady increase in the surface pressure and elastic modulus (Fig. 3a) as the proceeding island coalescence gets gradually the larger assemblies into contact. This accumulates stress at the assembly boundaries that is relieved by the nanoparticle re-arrangements into a continuous close-packed monolayer. A nearly unchanged Bragg rod maximum position and width (Fig. 3b,c) suggest that the local hexagonal order from the original islands is preserved. The nanoparticle Langmuir film at the end of stage II is completely closed, being suitable for the transfer onto a solid substrate to deposit a high-quality nanoparticle monolayer. In stage III, we observe a steeper increase in the surface pressure followed by a maximum in the surface elastic modulus which precedes a bilayer formation [3]. A shift in the Bragg rod maximum position to the higher q_y values suggests a decrease in the lattice spacing d_{10} by approximately 0.1 nm (Fig. 3b) while a simultaneous increase in the Bragg rod width (Fig. 3c) indicates a deterioration of the nanoparticle order due to the accumulated stress. Such a Bragg rod behaviour can be explained by a slight compressive deformation of the polymer surfactant capping the nanoparticles. This non-equilibrium compression phase has never been observed in the experiments under steady-state conditions. In stage IV, the peak P2 indicates a newly formed vertically correlated second nanoparticle layer allowing stress relief which results in the reversed shift of the Bragg rod maximum position and increase in the d_{10} lattice spacing. The Bragg rod width increases as well suggesting growing disorder. Such a simultaneous growth of the lattice spacing and disorder is typical for the paracrystal model [4]. In the limit of a highly disorder paracrystal, the Bragg rod maximum position is controlled by the interparticle distance instead the lattice spacing d_{10}, i.e. $q_y^{\max}$ 2 / instead $q_y^{\max}$ 2 / d_{10}. The $q_y^{\max}$ at the end of stage IV is in between that suggests a partial paracrystalline disorder. The Bragg rod maximum position and width are not recovered during the film expansion suggesting a stable nanoparticle order in the bilayer. The drop in the *P*2 peak area may be explained by decreasing amount of nanoparticles in the probed X-ray volume during the film expansion when the bilayer islands are formed and go away from each other, leaving free subphase surface behind (see also Fig. 2).

Conclusions

We identified principal stages of the Ag nanoparticle Langmuir film formation using the fast *in-situ* GISAXS technique supported by Brewster angle microscopy and imaging ellipsometry. The nanoparticle monolayer formation takes place via coalescence of free self-assembled nanoparticle islands with the hexagonal close-packed order that persists in the coalesced assemblies up to a temporary squeezing of the lattice shortly before the monolayer. This transient phase has not been observed under steady-state conditions. The monolayer collapse takes place by flipping up the nanoparticles and the second layer formation with the AB-like crystallographic stacking and enhanced paracrystalline-like disorder. The Langmuir film expansion runs irreversibly by decomposition into bilayer islands without observable changes in the nanoparticle order inside, leaving free subphase surface behind.

References

1. K. Vegso, P. Šiffalovič, M. Weis, M. Jergel, M. Benkovičová, E. Majková, L. Chitu, Y. Halahovets, Š. Luby, I. Capek & A. Šatka, *Phys. Stat. Sol.*, **A 208**, (2011), 2629-2634.
2. M. Fukuto; R. K. Heilmann, P. S. Pershan, A. Badia & R. B. Lennox, *J. Chem. Phys.*, **120**, (2004), 3446-3459.
3. S. Kubowicz, M. A. Hartmann, J. Daillant, M. K. Sanyal, V. V. Agrawal, C. Blot, O. Konovalov & H. Mo¨hwald, *Langmuir*, **25**. (2008), 952-958.
4. R. Lazzari, R., in *X-ray and Neutron Reflectivity*, edited by J. Daillant & A. Gibaud (Berlin-Heidelberg: Springer), 2009, pp 283-342.

Acknowledgement

This work was done during implementation of the project Research and Development Centre for Advanced X-ray Technologies, ITMS code 26220220170, supported by the Research and Development Operational Programme funded by the ERDF.

L7

GROWTH AND STRUCTURE OF THIN FILMS OF ORGANIC SEMICONDUCTORS: A REAL-TIME IN SITU GISAXS STUDY

C. Frank[1], J. Novák[1], R. Banerjee[1], A. Gerlach[1], F. Schreiber[1], A. Vorobiev[2], J. Banerjee[3], and S. Kowarik[3]

[1]Institut für Angewandte Physik, Eberhard Karls Universität Tübingen, Auf der Morgenstelle 10, 72076 Tübingen, Germany
[2]European Synchrotron Radiation Facility, 6 Rue Jules Horowitz, BP 220, 38043 Grenoble Cedex 9, France
[3]Institut für Physikalische und Theoretische Chemie, Universität Tübingen, Auf der Morgenstelle 18, 72076 Tübingen, Germany
[4]Institut für Physik, Humboldt University of Berlin, Newtonstr. 15, 12489 Berlin, Germany
frank.schreiber@uni-tuebingen.de

Recently, organic semiconductors (OSC) have attracted significant attention due to their applicability in electronic and optical devices [1]. The physical properties (e.g. optical absorption and conductivity) of OSC can be easily tuned by changing chemical groups or by fluorination. Additionally, low growth temperature of OSC thin films and their synthesis via chemical route results in low production-costs. The mechanical flexibility of OSC is another advantage in comparison to inorganic semiconductors.

Due to their non-trivial shape and molecular interactions, OSC demonstrate complex growth behaviour during thin film growth. This can include, e.g., rapid roughening and thickness dependent lattice parameters and lateral grain size [2, 3]. Since some of these effects may be transient, real-time *in situ* experiments during the film growth are necessary to understand these phenomena.

We present a combined grazing incidence small angle X-ray scattering (GISAXS) and X-ray specular reflectivity (XRR) real-time *in situ* study on growth of organic thin films of rod-like organic semiconductor molecule diindenoperylene (DIP, $C_{32}H_{16}$). The thin films were grown in a portable ultra-high vacuum chamber [4] allowing control of the substrate temperature and the growth rate, which were varied in ranges 25 – 100 ^{o}C and 0.1 – 1.1 nm/min, respectively. Synchrotron real-time measurements were performed at the ID10B beam-line of the ESRF (Grenoble, France) at a wavelength of 0.929 Å and an incidence angle of $_{i}$ = 0.8^{o}, which corresponds to the anti-Bragg point of the standing phase of DIP. The Maxipix single-photon counting 2D detector was used to monitor the GISAXS diffuse scattering in the vicinity of the Yoneda wing as well as the secularly reflected beam si-

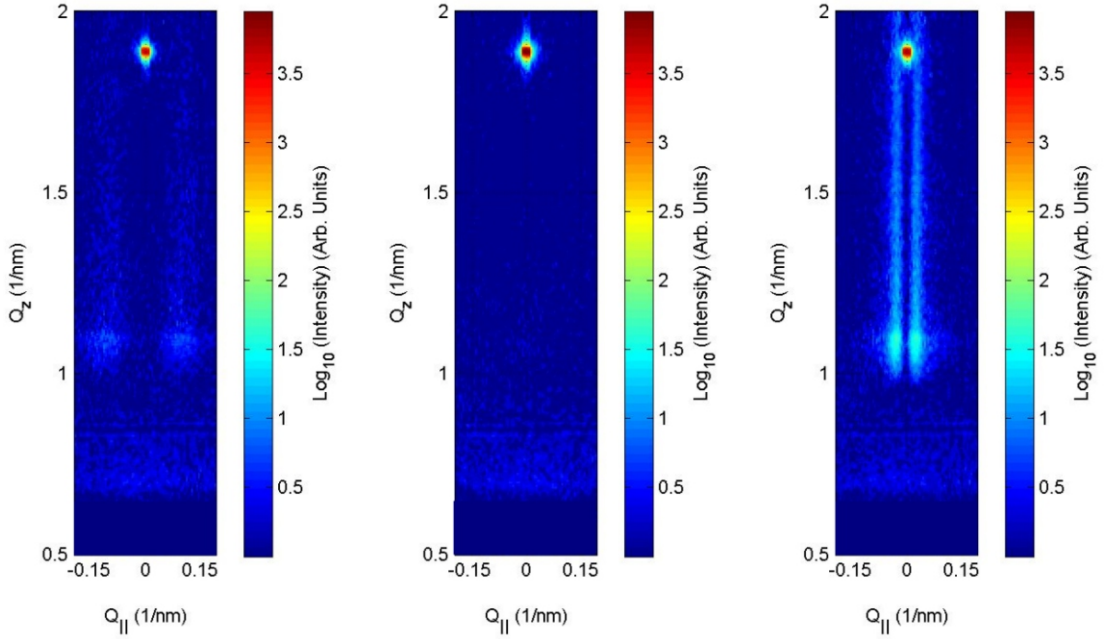

Figure 1. GISAXS images taken during the growth of a diindenoperilene (DIP) film at thicknesses of 0.5, 1.0 and 1.5 monolayers (left, middle, and right, respectively). The diffuse scattering present in left and right images is due to the presence of DIP molecular islands. Almost no diffuse scattering is present at 1.0 monolayer of DIP, since the layer is completed and no islands are present. The enhancement of intensity at Q_z=1.05 nm^{-1} corresponds to the Yoneda wing of the thin film. The intense peak around Q_z=1.9 nm^{-1} is the specular reflection from the sample at the anti-Bragg point of DIP standing phase

multaneously. The real-time measurements are complemented by post-growth AFM and XRR measurements.

The out-of-plane thickness dependent structure of the thin films, including the coverage of molecular layers and out-of-plane lattice constant, is probed using XRR measurements at the anti-Bragg condition. We apply a growth model first proposed by Trofimov et al. [5] in combination with kinematical scattering theory [6] to simulate the XRR data. Additionally, we need to implement thickness dependent lattice constant to fully describe the experimental observations. The detailed analysis reveals the layer-by-layer growth mode in the first two molecular layers and an onset of the film roughening from the third monolayer onwards. Additionally, we observe change of the out-of-plane lattice spacing and concomitant change of molecular tilt during the growth of the $2^{nd} - 4^{th}$ monolayer.

The in-plane structure of the thin films is probed using GISAXS measurements (see Fig. 1), which allow for determining thickness dependent distance of molecular islands and their size. We use the temperature dependence of the island size to determine effective activation energy of island nucleation in different layers. The effective energy in the 2^{nd} layer is smaller than that in the 1^{st} layer. The difference in activation energies explains the fact that islands grow smaller in the 1^{st} layer than in the 2^{nd} layer as observed using GISAXS and also in AFM post-growth images.

In conclusion, combined *in situ* real-time GISAXS and XRR measurements bring insight into the growth of the first few monolayers of DIP thin films. In particular, we are able to capture the transition from layer-by-layer growth to the thin film roughening and the change of lattice parameters during the growth and to identify difference in activation energies for the first two molecular layers.

1. Physics of Organic Semiconductors, edited by W. Brütting (Wiley-VCH, Weinheim, 2005).
2. S. Kowarik, A. Gerlach, S. Sellner, F. Schreiber, L. Cavalcanti, and O. Konovalov, *Phys. Rev. Lett*., **96**, (2006), 125504.
3. R. Banerjee, J. Novák, C. Frank, C. Lorch, A. Hinderhofer, A. Gerlach, and F. Schreiber, *Phys. Rev. Lett*., **110**, (2013), 185506.
4. K. A. Ritley, B. Krause, F. Schreiber, and H. Dosch, *Rev. Sci. Instrum*., **72**, (2001), 1453.
5. V. I. Trofimov and V. G. Mokerov, *Thin Solid Films*, **428**, (2003), 66.
6. S. Kowarik, A. Gerlach, M. W. A. Skoda, S. Sellner, and F. Schreiber, *Europ. Phys. J.- Special Topics*, **167**, (2009), 11.

We gratefully acknowledge the financial support of the DFG. We also acknowledge J. Krug (University Köln) and S. Bommel (Humboldt University Berlin) for helpful discussions and F. Anger (University Tübingen) for help during experiments.

Session III, Wednesday - morning, September 11

L9

SMALL-ANGLE NEUTRON SCATTERING CONTRIBUTION TO DEVELOPMENT OF SOME NOVEL MATERIALS

P. Strunz[1], D. Mukherji[2], M. Petrenec[3], R. Gilles[4], G. Schumacher[5], G. Pigozzi[6], U. Keiderling[5], T. Geue[7], U. Gasser[7], J. Šaroun[1] and J. Rösler[2]

[1]Nuclear Physics Institute ASCR, CZ-25068 Řež near Prague, Czech Republic
[2]TU Braunschweig, Institut für Werkstoffe, Langer Kamp 8, 38106 Braunschweig, Germany,
[3]IPM Brno, Czech Republic and TESCAN, a.s., Czech Republic
[4]TU München, Forschungsneutronenquelle Heinz Maier-Leibnitz (FRM II), Lichtenbergstraße 1, 85747 Garching, Germany
[5]Helmholtz Centre Berlin for Materials and Energy GmbH, Glienickerstr. 100, D-14109 Berlin, Germany
[6]Laboratory for Corrosion and Materials Integrity, EMPA Duebendorf, Switzerland
[7]Laboratory for Neutron Scattering, Paul Scherrer Institute, CH-5232 Villigen, Switzerland
strunz@ujf.cas.cz

Basic advantages and disadvantages of neutron radiation and its interaction with matter - with respect to materials research by means of neutron diffraction - are listed. The areas of Small-Angle Neutron Scattering (SANS) [1] application in materials science are discussed.

Several examples of the use of SANS to microstructural characterization of technologically important metallic materials are shown. First, a contribution of in-situ SANS to a solution of an open question in INCONEL polycrystalline superalloy load characteristics is reported. Secondly, evolution of ′-precipitate morphology in pre-deformed single-crystal Ni-base superalloy at elevated temperatures is determined. Afterwards, characterization of a porous membrane prepared by selective phase dissolution process from the single-crystal Ni superalloy is presented. Further, SANS characterization of Ni_3Si-type nanoparticles dispersed in a mixture of H_2O/D_2O using the contrast variation method is shown. Finally, the investigation of a model system (Al-Pb) for testing liquid-phase dispersion strengthening is discussed.